J|A|C|S
ARTICLES
Published on Web 04/20/2002

Carbon-13 NMR Shielding in the Twenty Common Amino Acids: Comparisons with Experimental Results in Proteins

Haihong Sun,[†] Lori K. Sanders,[‡] and Eric Oldfield*,[†,‡]

Contribution from the Departments of Biophysics and Chemistry, University of Illinois at Urbana-Champaign, 600 South Mathews Avenue, Urbana, Illinois 61801

Received July 31, 2001

Abstract: We have used ab initio quantum chemical techniques to compute the $^{13}C^{\alpha}$ and $^{13}C^{\beta}$ shielding surfaces for the 14 amino acids not previously investigated (R. H. Havlin et al., *J. Am. Chem. Soc.* **1997**, *119*, 11951−11958) in their most popular conformations. The spans ($\Omega = \sigma_{33} - \sigma_{11}$) of all the tensors reported here are large (≈34 ppm) and there are only very minor differences between helical and sheet residues. This is in contrast to the previous report in which Val, Ile and Thr were reported to have large (∼12 ppm) differences in Ω between helical and sheet geometries. Apparently, only the β-branched (β-disubstituted) amino acids have such large CSA span (Ω) differences; however, there are uniformly large differences in the solution-NMR-determined CSA ($\Delta\sigma^* = \sigma_{orth} - \sigma_{par}$) between helices and sheets in all amino acids considered. This effect is overwhelmingly due to a change in shielding tensor orientation. With the aid of such shielding tensor orientation information, we computed $\Delta\sigma^*$ values for all of the amino acids in calmodulin/M13 and ubiquitin. For ubiquitin, we find only a 2.7 ppm rmsd between theory and experiment for $\Delta\sigma^*$ over an ∼45 ppm range, a 0.96 slope, and an $R^2 = 0.94$ value when using an average solution NMR structure. We also report C^{β} shielding tensor results for these same amino acids, which reflect the small isotropic chemical shift differences seen experimentally, together with similar C^{β} shielding tensor magnitudes and orientations. In addition, we describe the results of calculations of C^{α}, C^{β}, C^{γ_1}, C^{γ_2}, and C^{δ} shifts in the two isoleucine residues in bovine pancreatic trypsin inhibitor and the four isoleucines in a cytochrome *c* and demonstrate that the side chain chemical shifts are strongly influenced by χ_2 torsion angle effects. There is very good agreement between theory and experiment using either X-ray or average solution NMR structures. Overall, these results show that both C^{α} backbone chemical shift anisotropy results as well as backbone and side chain ^{13}C isotropic shifts can now be predicted with good accuracy by using quantum chemical methods, which should facilitate solution structure determination/refinement using such shielding tensor surface information.

Introduction

There has recently been increased interest in computing ^{13}C, ^{15}N, and ^{19}F NMR chemical shifts in amino acids, peptides, and proteins.[1−4] This work was brought about in part by the experimental observation[5,6] that ^{13}C NMR chemical shifts of C^{α}, C^{β}, and C^{o} reflect in a general way the presence of secondary structure (α-helices and β-sheet regions) in proteins, and more recently, both solution[7] and solid-state NMR methods[8,9] have been used to determine chemical shift (or shielding) tensor information, in both peptides and proteins. To more fully utilize this information, it is necessary to deduce relationships between structure (ϕ,ψ,χ) and experimental shift or shift/shielding tensor results. Then, chemical shift, chemical shift tensor magnitude, and chemical shift tensor orientation information can all be used in protein or peptide structure prediction and refinement. In early work, we found that ab initio quantum chemical (primarily Hartree−Fock) methods permitted the successful prediction of isotropic chemical shifts in proteins[1] and shift or shielding tensor information in amino acids,[10] and we and others have reported additional related results more recently in both peptides and proteins.[3,4,9,11] An earlier theoretical investigation revealed that there appeared to be significant differences in $^{13}C^{\alpha}$ shielding tensor spans ($\Omega = \sigma_{33} - \sigma_{11}$, where σ_{ii} are the principal components of the chemical shielding tensor and $\sigma_{33} \geq \sigma_{22} \geq \sigma_{11}$) between helical and sheet geometries in the amino acids threonine, valine, and isoleucine,[11] whereas with glycine and alanine, helical and sheet tensor spans were about the same.

* To whom correspondence should be addressed. Telephone: (217) 333-3374. Fax: (217) 244-0997. E-mail: eo@chad.scs.uiuc.edu.
† Department of Biophysics.
‡ Department of Chemistry.

(1) de Dios, A. C.; Pearson J. G.; Oldfield, E. *Science* **1993**, *260*, 1491−1496.
(2) Oldfield, E. *J. Biomol. NMR* **1995**, *5*, 217−225.
(3) Sitkoff, D.; Case, D. A.; *Prog. NMR Spectrosc.* **1998**, *32*, 165−190.
(4) Xu, X. P.; Case, D. A. *J. Biomolec. NMR* **2001**, *21*, 321−333.
(5) Spera, S.; Bax. A. *J. Am. Chem. Soc.* **1991**, *113*, 5490−5492.
(6) Wishart, D. S.; Sykes, B.D. *J. Biomol. NMR.* **1994**, *4*, 171−180.
(7) Tjandra, N.; Bax, A. *J. Am. Chem. Soc.* **1997**, *119*, 9576−9577.
(8) Heller, J.; Laws, D. D.; King, D. S.; Wemmer, D. E.; Pines, A.; Havlin R. H.; Oldfield, E. *J. Am. Chem. Soc.* **1997**, *119*, 7827−7831.
(9) Havlin, R. H.; Laws, D. D.; Bitter H. L.; Sanders, L. K.; Sun, H.; Grimley, J. S.; Wemmer, D. E.; Pines, A.; Oldfield, E. *J. Am. Chem. Soc.*, **2001**, *123*, 10362−10369.
(10) de Dios, A. C.; Laws, D. D.; Oldfield, E. *J. Am. Chem. Soc.* **1994**, *116*, 7784−7786.
(11) Havlin, R. H.; Le, H.; Laws, D. D.; deDios A. C.; Oldfield, E. *J. Am. Chem. Soc.* **1997**, *119*, 11951−11958.

10.1021/ja011863a CCC: $22.00

However, using solution NMR spectroscopy, another measure of the chemical shift anisotropy, $\Delta\sigma^* = \sigma_{orth} - \sigma_{par}$, where σ_{par} represents the shielding along or parallel to the C−H bond vector and σ_{orth} represents the average shielding orthogonal to that direction, revealed that $\Delta\sigma^*$ values for helices were much smaller than $\Delta\sigma^*$ for sheet residues in the proteins ubiquitin and calmodulin.[7] Although much of the difference between the two "CSA" measurements, $\Delta\Omega$ and $\Delta\sigma^*$, can be attributed to changes in tensor orientation, it is clearly necessary to have a better understanding of the full tensor magnitudes and orientations in all amino acids, not just a small subset, in order to use such information in structure determination and refinement. Here, we present detailed theoretical results for the most popular conformations of the 14 amino acids not previously investigated in ref 11, and we discuss these new results together with those reported in the earlier work.[11] This information is also being provided at our web site, http://feh.scs.uiuc.edu and is also available in the Supporting Information and elsewhere.[12]

Experimental Section

Computational Methods. We have computed the $^{13}C^{\alpha}$ and $^{13}C^{\beta}$ shielding tensor surfaces for the following amino acids: cysteine (C), methionine (M), aspartic acid (D), asparagine (N), glutamic acid (E), glutamine (Q), leucine (L), lysine (K), arginine (R), histidine (H), phenylalanine (F), tyrosine (Y), and tryptophan (W), together with ψ shielding traces for proline (P), in addition to selected C^{α}, C^{β}, C^{γ_1}, C^{γ_2}, and C^{δ} calculations for isoleucine (I). In each case, the amino acid of interest was embedded in an *N*-formyl-L-amino acid amide molecule following our previous practice,[11] as shown, for example, for the C, K, W, and P species below.

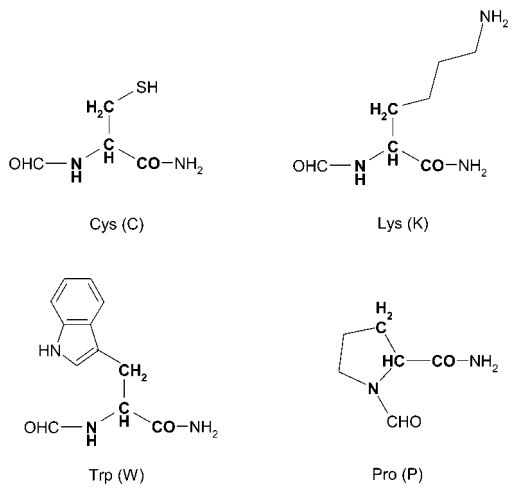

The basic side chain geometries chosen were the most abundant forms present in proteins, as reported from protein structure database searches.[13,14] In this study, only neutral species were investigated. We used Hartree−Fock (HF) theory in the Gaussian-98 program[15] and the gauge-including atomic orbitals (GIAO) method[16−18] to compute C^{α} and C^{β} shieldings. The general methods used were the same as those described previously for Gly, Ala, Val, Ile, Ser, and Thr[11] and included an initial energy minimization of bond lengths and three atom angles with a steepest descents algorithm, that is, the geometries present in an Amber[19] force field. Ab initio geometry optimization as well as the effects of using density functional theory methods has been studied by us previously in valine,[20] and the use of such geometry-optimized structures or DFT methods has only a very small effect on the shieldings observed. We used a locally dense[21] basis set in the coupled Hartree−Fock shielding calculations, 6-311++G(2d,2p), on the bold atoms shown above, with a 6-311G basis on the other atoms, where the notations refer to the basic basis sets of Pople and co-workers,[22] as implemented in Gaussian-98.[15] For the isoleucine side chains, a more extended locally dense basis was used, as described below.

Results and Discussion

We computed the C^{α} and C^{β} shielding tensor surfaces as a function of the peptide backbone torsion angles ϕ and ψ, $\sigma_{ii}C^{\alpha}(\phi,\psi)$ and $\sigma_{ii}C^{\beta}(\phi,\psi)$, for each of the 13 amino acids listed above, together with additional data, $\sigma_{ii}(\psi)$, for proline (the most abundant form for proline is "C^{γ} endo", so ϕ is fixed, and we only computed shielding tensors as a function of ψ). The chemical shielding tensor is a symmetric, second-rank tensor and can thus be described by three principal components: σ_{11}, σ_{22}, and σ_{33} and their orientations. The isotropic chemical shielding, σ_i, is given by $\sigma_i = 1/3\ \mathrm{Tr}\sigma = 1/3(\sigma_{11} + \sigma_{22} + \sigma_{33})$ and by convention is reported in parts per million from the bare ^{13}C nucleus. Some typical results for the aromatic amino acid tyrosine are shown in Figure 1, where we show $\sigma_i = \sigma_{isotropic}$ (Figure 1A), σ_{11} (Figure 1B), σ_{22} (Figure 1C), and σ_{33} (Figure 1D), all as a function of ϕ,ψ. The numbers on the surfaces are the absolute shieldings (σ_i, σ_{ii}) from the bare ^{13}C nucleus. Generally, similar results are obtained for all amino acids. The actual computed $^{13}C^{\alpha}$ shieldings, $\sigma_{ii}(\phi,\psi)$, for all amino acids are given in the Supporting Information and are also available from the Web (http://feh.scs.uiuc.edu and ref 12).

To facilitate discussion, the magnitudes of the shielding tensor elements σ_{11}, σ_{22}, and σ_{33}, together with the isotropic shielding, σ_i, for the 13 amino acids not investigated in detail previously, are shown in Table 1 (except proline, which is available in the Supporting Information), for typical helical and sheet geometries. From Table 1, it can be seen that the expected[5] increased ^{13}C NMR shielding of sheet over helical C^{α} residues is evident in all cases. Sheet residues are more shielded on average by 4.2 ppm, with a standard deviation of only 0.6 ppm. In contrast, for C^{β} (Table 2) sheet residues are now more deshielded by 1.5 ± 0.5 ppm. This is the behavior seen experimentally[5] and also noted in previous theoretical work on G,A,V,I,S, and T.[11]

What comes as a surprise, however, is that the tensor spans ($\Omega = \sigma_{33} - \sigma_{11}$) are extremely similar between helical and sheet

(12) R. H. Havlin, Chemical Shielding Calculator, http:// waugh.cchem.berkeley.edu/∼bob/cs.html
(13) Ponder, J. W.; Richards, F. M. *J. Mol. Biol.* **1987**, *193*, 775−791.
(14) Lovell, S. C.; Word, J. M.; Richardson, J. S.; Richardson, D. C.; *Proteins* **2000**, *40*, 389−408.
(15) Frisch, M. J.; Trucks, G. W.; Schlegel, H. B.; Scuseria, G. E.; Robb, M. A.; Cheeseman, J. R.; Zakrzewski, V. G.; Montgomery, J. A., Jr.; Stratmann, R. E.; Burant, J. C.; Dapprich, S.; Millam, J. M.; Daniels, A. D.; Kudin, K. N.; Strain, M. C.; Farkas, O.; Tomasi, J.; Barone, V.; Cossi, M.; Cammi, R.; Mennucci, B.; Pomelli, C.; Adamo, C.; Clifford, S.; Ochterski, J.; Petersson, G. A.; Ayala, P. Y.; Cui, Q.; Morokuma, K.; Malick, D. K.; Rabuck, A. D.; Raghavachari, K.; Foresman, J. B.; Cioslowski, J.; Ortiz, J. V.; Baboul, A. G.; Stefanov, B. B.; Liu, G.; Liashenko, A.; Piskorz, P.; Komaromi, I.; Gomperts, R.; Martin, R. L.; Fox, D. J.; Keith, T.; Al-Laham, M. A.; Peng, C. Y.; Nanayakkara, A.; Gonzalez, C.; Challacombe, M.; Gill, P. M. W.; Johnson, B.; Chen, W.; Wong, M. W.; Andres, J. L.; Gonzalez, C.; Head-Gordon, M.; Replogle, E. S.; Pople, J. A. *Gaussian 98*, Revision A.7.; Gaussian, Inc.: Pittsburgh, PA, 1998.
(16) London, F. *J. Phys. Radium* **1937**, *8*, 397−409.
(17) Ditchfield, R. *J. Chem. Phys.* **1972**, *56*, 5688−5691.
(18) Pulay, P.; Hinton, J.F. *Encycl. Nucl. Magn. Reson.* **1996**, 4334−4339.
(19) Weiner, S. J.; Kollman, P. A.; Case, D. A.; Singh, U. C.; Ghio, C.; Alagona, G.; Profeta, S. Jr.; Weiner, P**.** *J. Am. Chem. Soc.* **1984**, *106*, 765−784. Weiner, S. J.; Kollman, P. A.; Nguyen, D. T.; Case, D. A. *J. Comput. Chem*. **1986**, *7*, 230−252.
(20) Pearson J. G.; Le, H.; Sanders, L. K.; Godbout, N.; Havlin, R. H.; Oldfield, E. *J. Am. Chem. Soc.* **1997**, *119*, 11941−11950.
(21) Chestnut, D. B.; Moore, K. D. *J. Comput. Chem*. **1989**, *10*, 648−659.
(22) Hehre, W. J.; Radom, L.; Schleyer, P.; Pople, J. A. *Ab Initio Molecular Orbital Theory*; John Wiley and Sons: New York, 1986.

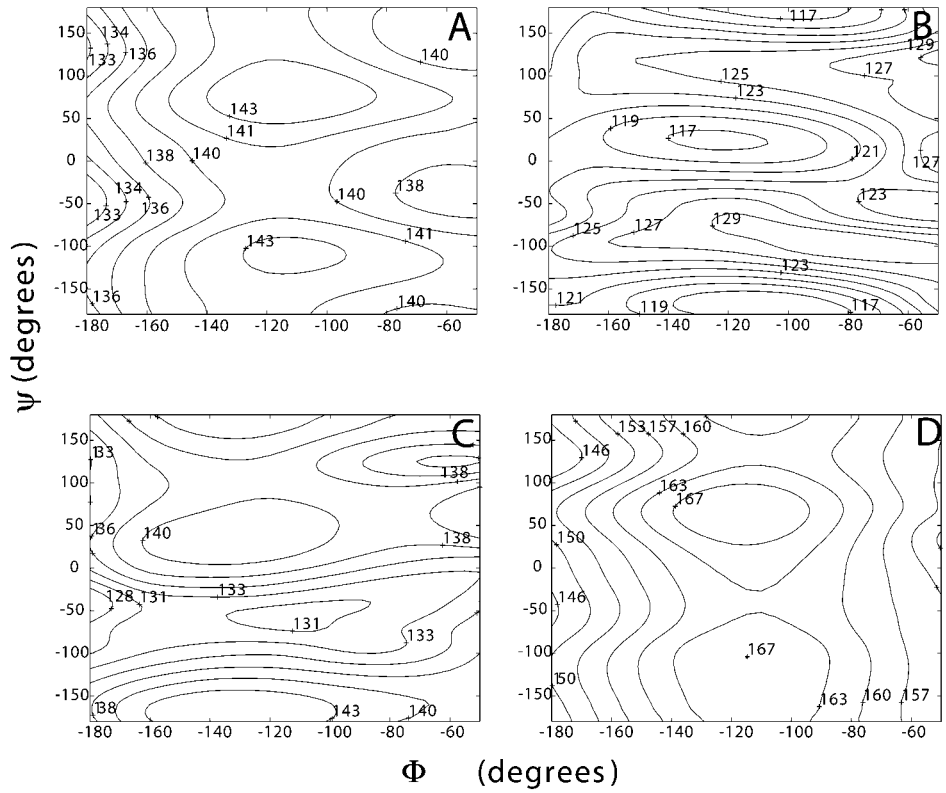

Figure 1. Computed isotropic shielding and anisotropic shielding tensor element surfaces for $^{13}C^{\alpha}$ in *N*-formyl tyrosine amide ($\chi_1 = -60°$, $\chi_2 = -85°$): (A) σ_{iso}, (B) σ_{11}, (C) σ_{22}, and (D) σ_{33}.

Table 1. Summary of Representative Computed $^{13}C^{\alpha}$ Shielding Tensors for Several *N*-Formyl Amino Acid Amide Peptide Model Systems

		shielding (ppm)							
system	structure[a]	σ_{11}	σ_{22}	σ_{33}	σ_i	Ω^b	$(\sigma_i^S - \sigma_i^h)^c$	$\Delta\Omega^d$	$\Delta\sigma^*$
cys	helix ($\chi_1 = -60°$)	117.5	134.2	157	136.2	39.6	5.2	3.3	−2.7
	sheet	124.8	131.7	167.6	141.4	42.9			24.3
met	helix ($\chi_1 = -65°$, $\chi_1 = -65°$, $\chi_1 = -70°$)	133	143.2	160.8	145.7	27.8	3.3	7.2	2.3
	sheet	130.4	151	165.5	149	35			27.6
asp	helix ($\chi_1 = -70°$, $\chi_2 = -15°$)	129.6	144.6	159.9	144.7	30.3	4.3	−1.0	−2.4
	sheet	135	147.8	164.3	149	29.3			20.6
asn	helix ($\chi_1 = -65°$, $\chi_2 = -20°$)	130.1	145.2	160.5	145.2	30.4	4.3	−0.3	−1.2
	sheet	134.8	148.5	165	149.5	30.1			21.6
glu	helix ($\chi_1 = -60°$, $\chi_2 = 180°$, $\chi_3 = -10°$)	129.1	142.6	157.2	143	28.1	4.4	5.9	−1.8
	sheet	131.2	146	165.1	147.4	34			24
gln	helix ($\chi_1 = -60°$, $\chi_2 = 180°$, $\chi_3 = -30°$)	128.3	142.3	157.3	142.6	29	4.1	5.3	−2.8
	sheet	130.5	145.0	164.8	146.7	34.3			23.7
lys	helix ($\chi_1 = -60°$, $\chi_2 = 180°$, $\chi_3 = 180°$, $\chi_4 = 180°$)	126.7	140.1	156.6	141.1	29.9	4.3	6.5	−2.4
	sheet	128.5	142.7	164.9	145.4	36.4			24.1
arg	helix ($\chi_1 = -67°$, $\chi_2 = 180°$, $\chi_3 = 180°$, $\chi_4 = 180°$)	126.7	140	155.7	140.8	29	4.3	6.1	−3.3
	sheet	129.1	142.1	164.2	145.1	35.1			22.7
his	helix ($\chi_1 = -65°$, $\chi_2 = -70°$)	128.5	140.5	158.6	142.5	30.1	3.4	2.9	−4
	sheet	130.4	143.9	163.4	145.9	33			22.6
phe	helix ($\chi_1 = -65°$, $\chi_2 = -85°$)	117.7	134.3	152.4	134.8	34.7	5.4	−0.6	−5
	sheet	125.1	136.2	159.2	140.2	34.1			21.6
tyr	helix ($\chi_1 = -60°$, $\chi_2 = -85°$)	122.7	134.7	155.8	137.7	33.1	5.3	4.0	−3.6
	sheet	126.1	139.7	163.2	143.0	37.1			24.7
trp	helix ($\chi_1 = -65°$, $\chi_2 = 95°$)	126.5	141.4	159.1	142.3	32.6	3.7	4.4	−3.2
	sheet	129	143	166	146	37			25.5
leu	helix ($\chi 1 = -60°$, $\chi_2 = 180°$)	131.4	141.2	159.5	144.1	28.1	3.5	6.7	1.3
	sheet	129.5	148.8	164.3	147.6	34.8			26.8
Average	helix					30.4	4.3	3.9	−2.4
	sheet					33.6			23.6

[a] Helix means $\phi = -60°$, $\psi = -60°$; sheet means $\phi = -120°$, $\psi = 120°$. Full surfaces are provided in the Supporting Information. [b] $\Omega = \sigma_{33} - \sigma_{11}$. [c] The helix−sheet isotropic chemical shift separation: the helices are less shielded. [d] $\Delta\Omega = \Omega^{sheet} - \Omega^{helix}$.

geometries. For example, the value of $\Delta\Omega = \Omega^{sheet} - \Omega^{helix}$ is on average only 3.9 ppm, with a standard deviation of 2.8 ppm (Table 1). Helices and sheets have essentially the same CSA and Ω, contrary to the general conclusions drawn previously from similar calculations on valine, isoleucine, and threonine, in which sheet residues typically had much larger Ω values than did residues in α-helical geometries.[11] For C^{β}, the sheet residues are on average ∼1.5 (± 0.5) ppm downfield of the helical

Table 2. Summary of Overall Computed $^{13}C^{\beta}$ NMR Shielding Tensor Breadths and Isotropic Shielding Differences for Various *N*-Formyl Amino Acid Peptide Model Systems in Helical and Sheet Geometries

		shielding (ppm)						
system	structure[a]	σ_{11}	σ_{22}	σ_{33}	σ_i	Ω^b	$(\sigma_i^s - \sigma_i^h)^c$	$\Delta\Omega^d$
cys	helix ($\chi_1 = -60°$)	148.5	166.4	178.0	164.3	29.6		
	sheet	142.5	166.8	175.5	161.6	33.0	−2.7	3.4
met	helix ($\chi_1 = -65°, \chi_1 = -65°, \chi_1 = -70°$)	152.9	168.3	177.1	166.1	24.2		
	sheet	152.5	165.7	175.8	164.7	23.3	−1.4	−0.9
asp	helix ($\chi_1 = -70°, \chi_2 = -15°$)	139.1	153.2	175.4	155.9	32.3		
	sheet	137.6	152.5	173.1	154.4	35.6	−1.5	3.3
asn	helix ($\chi_1 = -65°, \chi_2 = -20°$)	138.3	154.6	178.2	157.0	40.0		
	sheet	137.0	154.3	176.4	155.9	39.4	−1.1	−0.6
glu	helix ($\chi_1 = -60°, \chi_2 = 180°, \chi_3 = -10°$)	152.9	162.9	181.4	165.7	28.5		
	sheet	148.5	161.8	181.7	164.0	33.1	−1.7	4.6
gln	helix ($\chi_1 = -60°, \chi_2 = 180°, \chi_3 = -30°$)	154.0	163.8	181.0	166.3	27.0		
	sheet	149.2	162.8	181.2	164.4	31.9	−1.9	4.9
lys	helix ($\chi_1 = -60°, \chi_2 = 180°, \chi_3 = 180°, \chi_4 = 180°$)	145.9	158.9	176.7	160.5	30.8		
	sheet	141.3	160.2	1758	159.1	34.5	−0.6	3.7
arg	helix ($\chi_1 = -67°, \chi_2 = 180°, \chi_3$=180°, $\chi_4 = 180°$)	150.8	160.4	176.5	162.6	25.7		
	sheet	146.9	160.5	175.9	161.1	29.1	−1.5	4.4
his	helix ($\chi_1 = -65°, \chi_2 = -70°$)	151.0	164.7	172.5	162.7	21.5		
	sheet	147.3	164.3	172.4	161.3	25.1	−1.4	3.6
phe	helix ($\chi_1 = -65°, \chi_2 = -85°$)	147.8	149.3	170.9	156.0	23.1		
	sheet	144.2	151.5	167.7	154.5	23.5	−1.5	0.4
tyr	helix ($\chi_1 = -60°, \chi_2 = -85°$)	149.7	151.5	171.8	157.7	22.1		
	sheet	145.5	153.8	169.6	156.2	24.1	−1.5	2.0
trp	helix ($\chi_1 = -65°, \chi_2 = 95°$)	153.0	167.6	177.0	165.9	23.9		
	sheet	151.3	166.8	177.4	165.2	26.1	−0.7	2.2
leu	helix ($\chi_1 = -60°, \chi_2 = 180°$)	151.0	164.7	172.5	162.7	21.5		
	sheet	147.2	164.3	172.4	161.3	25.1	−1.4	3.6
av	helix					26.9		
	sheet					29.5	−1.5	2.7

[a] Helix means $\phi = -60°$, $\psi = -60°$; sheet means $\phi = -120°$, $\psi = 120°$. [b] $\Omega = \sigma_{33} - \sigma_{11}$. [c] The helix−sheet isotropic chemical shift separation: the helices are more shielded. [d] $\Delta\Omega = \Omega^{sheet} - \Omega^{helix}$.

residues, as expected,[5] and again the Ω values are very similar, with $\Delta\Omega = 2.7 \pm 1.9$ ppm (Table 2). These C^{α} results were quite unexpected, since in previous work on Val, Ile, Thr, and Ser, we found that on average $\Omega \sim 34$ ppm for C^{α} in sheet geometries but Ω was only ∼22 ppm in helical geometries, a 12 ppm difference.[11] This was previously attributed to the presence of a "β substitution", since Gly and Ala did not show this effect. However, with the availability now of data for all 20 amino acids, it is clear that only the *doubly* β-substituted or *β-branched* amino acids valine, isoleucine, and threonine, can have this small $^{13}C^{\alpha}$ chemical shift anisotropy, Ω. The similarity between the $^{13}C^{\alpha}$ Ω values is shown graphically in Figure 2 for the 13 newly calculated amino acids, results which are clearly quite different from those shown in Figure 2 of ref 11, where the $^{13}C^{\alpha}$ Ω values for Val, Ile, and Thr were on average ∼12 ppm smaller in helical geometries.[11]

Also of considerable interest in this context is the observation that in *solution*, NMR determinations of the "chemical shift anisotropy", defined[7] as $\Delta\sigma^* = \sigma_{orth} - \sigma_{par}$, where σ_{par} is the shielding parallel to the $C^{\alpha}-H^{\alpha}$ bond vector and σ_{orth} is the average value perpendicular to this direction, there are remarkably large and consistent differences between $\Delta\sigma^*$ for helical and sheet geometries—for all amino acids. For example, Tjandra and Bax[7] reported $\Delta\sigma^* \approx 6$ ppm for helical and $\Delta\sigma^* \approx 27$ ppm for sheet residues in the proteins ubiquitin and calmodulin. These trends appeared consistent with our earlier[11] Ω calculations of large sheet Ω values and generally small helix Ω values, but at first sight, these results might now appear inconsistent with the entire amino acid database.

Fortunately, these apparent differences can simply be attributed to the different definitions used for the CSA. In

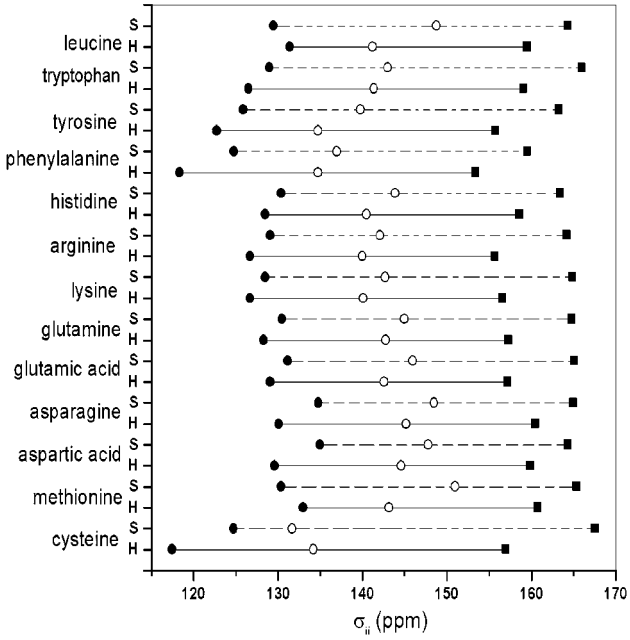

Figure 2. Diagram showing the shielding tensor elements, σ_{ii}, for each system investigated: ●, σ_{11}; ○, σ_{22}; ■, σ_{33}. The solid lines join the helical data sets; the broken lines join the sheet data sets.

computational chemistry, the principal components of the chemical shielding tensor are given by σ_{11}, σ_{22}, and σ_{33}, and in solid-state NMR, the principal components of the chemical shift tensor are given by δ_{11}, δ_{22}, and δ_{33}. In solid-state NMR, the principal components are typically extracted directly from NMR powder patterns or magic-angle sample-spinning line shapes, whereas in computational work, they are obtained by diago-

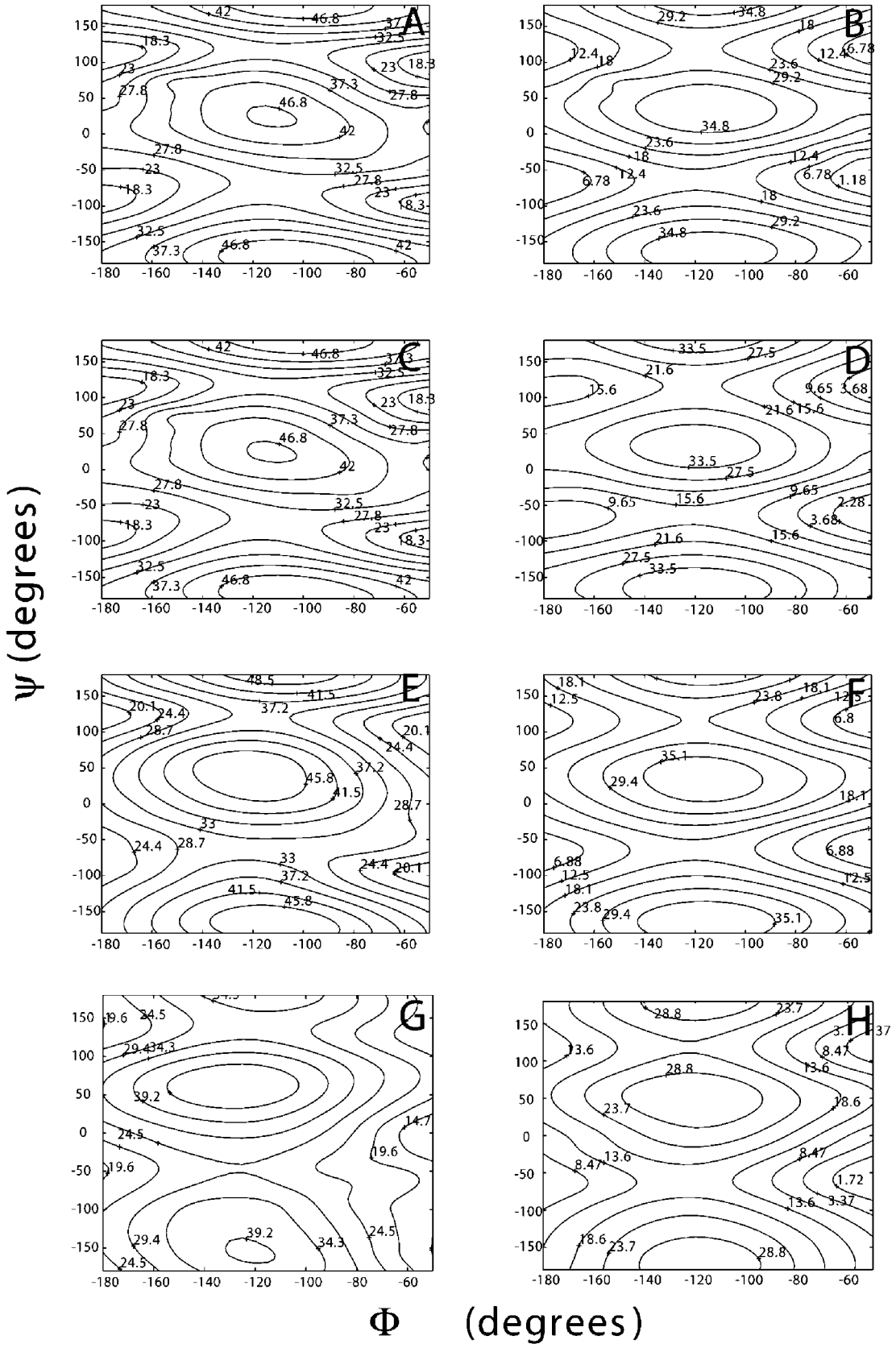

Figure 3. Computed span ($\Omega = \sigma_{33} - \sigma_{11}$) and solution NMR CSA ($\Delta\sigma^* = \sigma_{orth} - \sigma_{par}$) surfaces for $^{13}C^{\alpha}$ in *N*-formyl amino acid amides: (A) Ω, Ala; (B) $\Delta\sigma^*$, Ala; (C) Ω, Phe; (D) $\Delta\sigma^*$, Phe; (E) Ω, Glu; (F) $\Delta\sigma^*$, Glu; (G) Ω, Val ($\chi_1 = 180°$); (H) $\Delta\sigma^*$, Val ($\chi_1 = 180°$).

nalization of the full 3×3 chemical shielding tensor computed by using quantum chemistry. There is no orientational information in σ_{11}, σ_{22}, or σ_{33}. In contrast, in solution NMR, the cross correlation between relaxation due to $^{13}C^{\alpha}$—$^{1}H^{\alpha}$ dipolar and $^{13}C^{\alpha}$ chemical shift anisotropy interactions has been analyzed in terms of a symmetric tensor $\Delta\sigma^* = \sigma_{orth} - \sigma_{par}$, and the value of this

property is intimately related to the relative orientations of the C−H bond vector and the principal components of the shielding tensor. Thus, if the tensor changes orientation, there are relaxation changes, and these are reflected in potentially large changes in $\Delta\sigma^*$. Since full tensor orientations are obtained from the ab initio calculations and since such computed tensor orientation information was previously validated in the amino acid threonine,[10] a suitable transformation using the direction cosines of the shielding tensor, d_i, can be used to transform the principal components of the shielding tensor, σ_{11}, σ_{22}, and σ_{33}, into the reference frame used for the solution NMR experiments,

$$\sigma_{par} = [d_1 d_2 d_3]\begin{bmatrix}\sigma_{11} & 0 & 0\\ 0 & \sigma_{22} & 0\\ 0 & 0 & \sigma_{33}\end{bmatrix}\begin{bmatrix}d_1\\ d_2\\ d_3\end{bmatrix} \quad (1)$$

where σ_{ii} are the shielding tensor elements in the principal axis system and d_i are the direction cosines of the $C^\alpha-H^\alpha$ bond vector with respect to the principal axes of the shielding tensor. Once σ_{par} is determined, it is a trivial matter to obtain $\Delta\sigma^*$, since $\sigma_i = 1/3\ \mathrm{Tr}\ \tilde{\sigma} = 1/3(2\sigma_\perp + \sigma_\parallel)$.

To more clearly illustrate this, we show in Figure 3 $\Omega(\phi,\psi)$ and $\Delta\sigma^*(\phi,\psi)$ surfaces for alanine (Figure 3A,B), phenylalanine (Figure 3C,D), glutamic acid (Figure 3E,F) and valine ($\chi_1 = 180°$, Figure 3G,H). Close inspection reveals very similar Ω values for Ala, Phe, and Glu in helical and sheet regions (Figure 3A,C,E), a larger difference for Val ($\chi_1 = 180°$) (Figure 3G), and extremely large differences in $\Delta\sigma^*$ for all four amino acids (Figures 3B, D, F and H). These results typify the findings outlined in Table 1 and are consistent with those obtained previously.[11] For all non-β-branched amino acids, the CSA Ω values are both large and similar for helical and sheet geometries. For the β-branched amino acid valine, the Ω values are typically rather different, as noted in previous work on Val, Ile, and Thr.[11] However, in all cases, $\Delta\sigma^*$ values show large differences between helical and sheet geometries. These differences are overwhelmingly due to changes in the $^{13}C^\alpha$ shielding tensor orientation, as shown, for example, for $^{13}C^\alpha$ in lysine in Figure 4A,B. There is, however, essentially no change in the C^β tensor orientation between helical and sheet geometries, again as shown for example in the case of lysine in Figure 4C,D. The same lack of change in C^β tensor orientation between helical and sheet geometries was previously noted for the β-branched amino acid valine and is quite general.[11] The C^α tensor orientation results are of particular interest in the context of using $\Delta\sigma^*$ values in structure refinement, so we next consider them in more detail, followed by a comparison between experimental and quantum chemically predicted ^{13}C $\Delta\sigma^*$ values in calmodulin/M13 and ubiquitin.

In the helical geometries of all of the amino acids, σ_{22} is aligned close to the C−H bond vector and makes the major (~80%) contribution to shielding, followed by σ_{33} (~18%), as shown in Figure 5A. However, in sheet geometries, σ_{11} contributes ~96% to shielding along the C−H bond vector (Figure 5B), with σ_{22} making only a ~3% contribution. Of course, these results are solely for the idealized $\phi = -60°$, $\psi = -60°$ and $\psi = -120°$, $\psi = 120°$ geometries and are similar to those first reported by Walling et al.[23] However, with the availability of complete shielding surfaces (Supporting Information), it is now possible to see in detail how the tensor varies with ϕ,ψ, and typical results are shown for leucine in Figure 6. Figure 6A shows the orientation surface $\alpha_1(\phi,\psi)$ for α_1, the angle between σ_{11} and the C−H bond vector, Figure 6B shows the orientation surface α_2 (ϕ,ψ), where α_2 is the angle between σ_{22} and the C−H bond vector, and Figure 6C shows the α_3 (ϕ,ψ) surface, where α_3 is the angle between σ_{33} and the C−H bond vector. Clearly, none of the surfaces displays an $\alpha_i = 0$

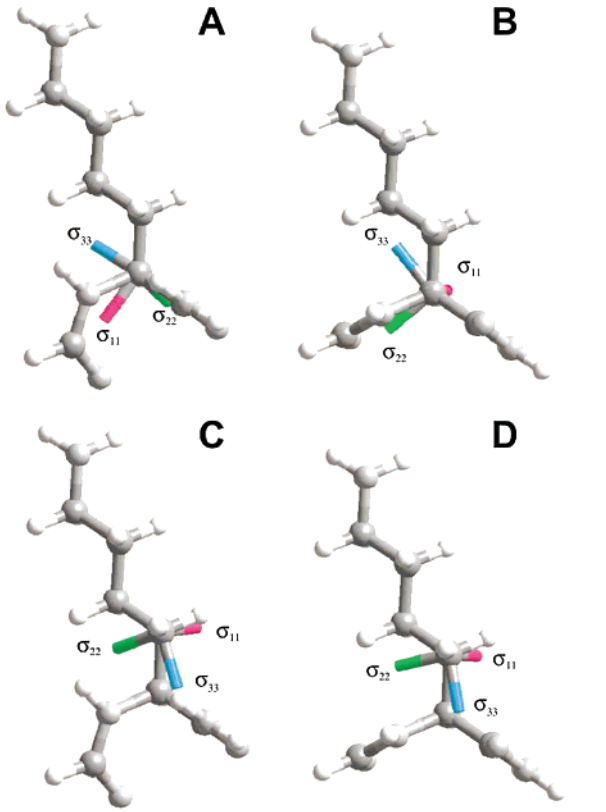

Figure 4. Orientation of principal components of the $^{13}C^\alpha$ and $^{13}C^\beta$ shielding tensors for lysine ($\chi_1 = -60°$, $\chi_2 = 180°$, $\chi_3 = 180°$, and $\chi_4 = 180°$): (A) C^α, helix; (B) C^α, sheet; (C) C^β, helix; and (D) C^β, sheet. Helix: $\phi = -60°$, $\psi = -60°$; sheet: $\phi = -120°$, $\psi = 120°$.

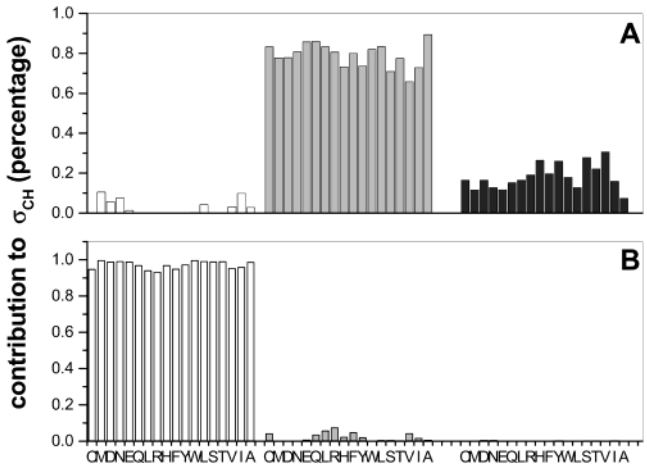

Figure 5. Graph showing contributions from the principal components of the $^{13}C^\alpha$ shielding tensor to shielding along the C−H bond vector: (A) sheet geometry, (B) helical geometry; σ_{11} (open), σ_{22} (gray), and σ_{33} (black). Letter codes for amino acids are given at the bottom of the figure. Results for 18 amino acids are shown; glycine and proline are omitted.

(23) Walling, A. E.; Pargas, R. E.; de Dios, A. C. *J. Phys. Chem. A* **1997**, *101*, 7299−7303.

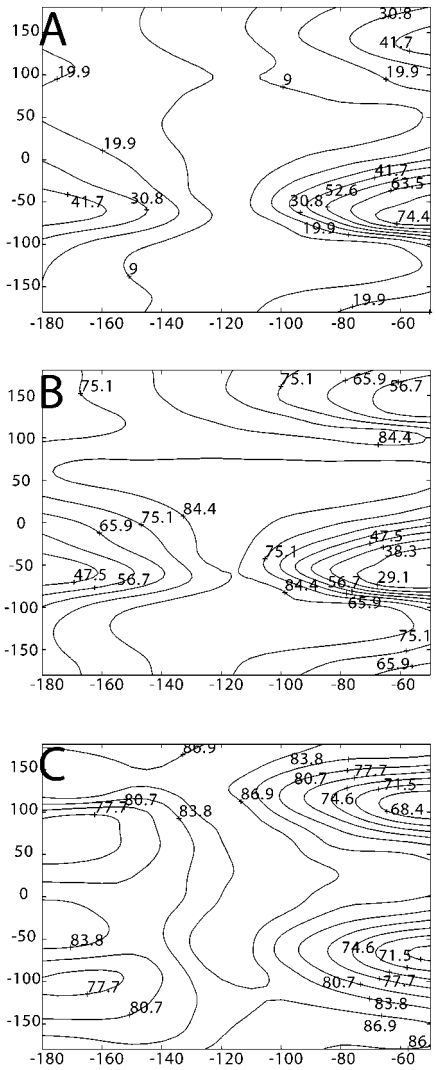

Figure 6. Computed $^{13}C^{\alpha}$ shielding tensor orientation surfaces for *N*-formyl leucine amide ($\chi_1 = -60°$, $\chi_2 = 180°$): (A) α_1, (B) α_2, and (C) α_3. α_1 is the angle between σ_{11} and the C−H bond vector; α_2 is the angle between σ_{22} and the C−H bond vector; α_3 is the angle between σ_{33} and the C−H bond vector.

contour, which would indicate perfect alignment of σ_{ii} and the C−H bond vector. Consequently, $\Delta\sigma^*$ is always < Ω. Overall, these theoretical results clearly indicate that large differences between helical and sheet CSAs ($\Omega = \sigma_{33} - \sigma_{11}$) are to be expected only for the β-branched amino acids valine, isoleucine, and threonine. They are also consistent with the recent solid-state ^{13}C NMR observation that both helical and sheetlike leucine residues in small peptides have large CSA (Ω) values.[9] The results shown in Table 1 do suggest somewhat larger Ω differences for the longer alkyl chain containing amino acids versus the shorter-chain ones (∼6 ppm on average for Met, Glu, Gln, Lys, Arg, and Leu versus ∼ 1 ppm for Cys, Asp, and Asn), although these effects are clearly minor when compared with the solution NMR $\Delta\sigma^*$ differences.

We next consider the experimental $\Delta\sigma^*$ results of Tjandra and Bax,[7] who investigated the proteins calmodulin/M13 and ubiquitin. In earlier work, Case and Sitkoff[3] found a 7 ppm rms error between theory and experiment for the $\Delta\sigma^*$ values in calmodulin/M13 and ubiquitin and those predicted theoretically using just alanine $^{13}C^{\alpha}$ shielding results, whereas we obtained somewhat smaller rmsd's using individual $^{13}C^{\alpha}$ shielding surfaces,[24] albeit with only a small subset of amino acid residues. To begin with, we consider $\Delta\sigma^*$ results for calmodulin/M13. Using ϕ,ψ torsions from the average solution NMR structure 2BBM,[25] the results predicted from an alanine surface are poor. The rmsd is 9.7 ppm, the slope is 0.67, and the R^2 value is 0.34 (Table 3). When using the X-ray crystal structure 1CDL,[26] there is a noticeable improvement to an rmsd of 6.3 ppm with a slope of 0.99 and an R^2 value = 0.72 (Table 3). When using individual $\Delta\sigma^*$ shielding surfaces for each amino acid, there is a further slight improvement, an rmsd of 8.9 ppm for the average solution NMR structure (slope = 0.72, $R^2 = 0.41$), and when using the calmodulin crystal structure, we find that the rmsd has decreased to 5.6 ppm, (slope = 0.94, $R^2 = 0.75$; Table 3). These errors are, however, large when compared to the ∼45 ppm total range in $\Delta\sigma^*$. There is a small improvement when using the individual $\Delta\sigma^*$ surfaces, but the largest improvement occurs when using the crystal structure. In sharp contrast to these results, with the much smaller protein ubiquitin (Figure 7 and Table 3), we find a 3.8 ppm rmsd using the average NMR structure 1D3Z[27] and the alanine surface, (slope = 0.89, $R^2 = 0.86$), whereas when using the X-ray structure 1UBQ,[28] we find an rmsd of 4.6 ppm (slope = 0.90, $R^2 = 0.81$). In this case, the solution NMR structure gives a clearly improved result over the X-ray structure, using just an alanine surface. And when the individual amino acid shielding surfaces are used, there is further improvement: For the NMR structure, we find that rmsd = 2.7 ppm, a slope = 0.96, and an $R^2 = 0.94$, whereas the X-ray structure shows that rmsd = 3.6 ppm, slope = 0.91, and $R^2 = 0.88$ (Figures 7C,D and Table 3). The average solution NMR structure of ubiquitin gives clearly improved results over the X-ray result, with the rmsd of 2.7 ppm being quite small when compared to the ∼45 ppm experimental range in $\Delta\sigma^*$. Thus, although the results with calmodulin show relatively poor correlations, the correlations with the much smaller protein ubiquitin (and those with model tripeptides[9]) are much better, implying that it should be possible to improve the calmodulin structure using $\Delta\sigma^*$ information. On the basis of these results, it appears that much of the variation between $\Delta\sigma^*$ values measured experimentally and those determined computationally arises from uncertainties in the structures that are used, since both peptide crystal and ubiquitin rms deviations are small, but those in the much larger calmodulin molecule are 2−3× larger. To study this question in more detail, we investigated any possible correlations between the rms error in $\Delta\sigma^*$ and protein structure quality (Figure 8). Here we plot the $\Delta\sigma^*$ rms error for five protein structures (ubiquitin: 1D3Z, 1UBI,[29] and 1UBQ; calmodulin: 1CDL and 2BBM) as a function of the percent residues outside the most favored regions of ϕ,ψ spaces, as determined by using the

(24) Szabo, C. M.; Sanders, L. K.; Arnold, W.; Grimley, J. S.; Godbout, N.; McMahon, M. T.; Moreno, B.; Oldfield, E. In *Modeling NMR Chemical Shifts—Gaining Insights into Structure and Environment;* Facelli, J. C., deDios, A. C., Eds.; ACS Symposium Series 732, **1999**, 40−62.
(25) Ikura, M.; Clore, G. M.; Gronenborn, A. M.; Zhu, G.; Klee, C. B.; Bax, A. *Science* **1992**, *256*, 632−638.
(26) Meador, W. E.; Means, A. R.; Quiocho, F. A. *Science* **1992**, *257*, 1251−1255.
(27) Cornilescu, G.; Marquardt, J. L.; Ottiger, M.; Bax, A. *J. Am. Chem. Soc.* **1998**, *120*, 6836−6837.
(28) Vijay-Kumar, S.; Bugg, C. E.; Cook, W. J. *J. Mol. Biol.* **1987**, *194*, 531−544.
(29) Alexeev, D.; Bury, S. M.; Turner, M. A.; Ogunjobi, O. M.; Muir, T. W.; Ramage, R.; Sawyer, L. *Biochem. J.* **1994**, *299*, 159−163.

Table 3. Statistical Results for $^{13}C^{\alpha}$ $\Delta\sigma^*$ Experimental/Theoretical Correlations in Calmodulin/M13 and Ubiquitin

		alanine surface			individual surface		
protein	structure	rmsd (ppm)	slope	R^2	rmsd (ppm)	slope	R^2
calmodulin/M13	2BBM(NMR)[a]	9.7	0.67	0.34	8.9	0.72	0.41
	1CDL (X-ray, 2.2 Å)[b]	6.3	0.99	0.72	5.6	0.94	0.75
ubiquitin	1D3Z (NMR)[c]	3.8	0.89	0.86	2.7	0.96	0.94
	1UBQ (X-ray, 1.8 Å)[d]	4.6	0.90	0.81	3.6	0.91	0.88

[a] From ref 25. [b] From ref 26. [c] From ref 27. [d] From ref 28.

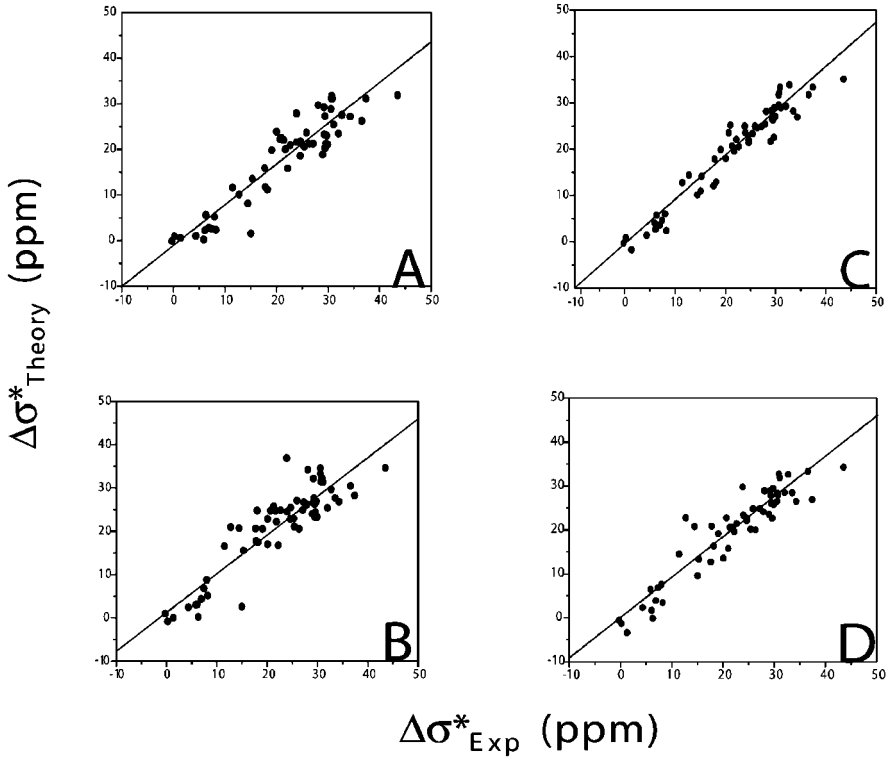

Figure 7. Correlations between experimental and computed $\Delta\sigma^*$ values in ubiquitin: (A) NMR/Ala, (B) X-ray/Ala, (C) NMR/individ, and (D) X-ray/individ. NMR, average solution NMR structure used; Ala, alanine C^{α} shielding surface used; and individ, an individual C^{α} shielding surface used. For the statistics, see Table 3.

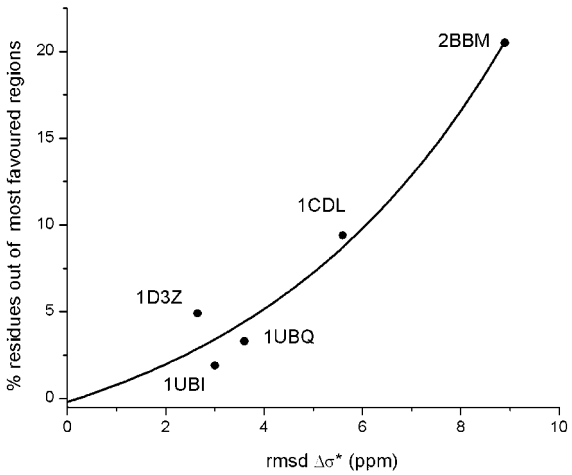

Figure 8. Graph showing relation between $\Delta\sigma^*$ (rsm error between the experimental $\Delta\sigma^*$ and that computed from the structure indicated) and the quality (percent residues outside the most favored regions) of the protein structure. Ubiquitin: 1UBI,[29] 1UBQ[28] and 1D3Z;[27] calmodulin: 1CDL[26] and 2BBM.[25]

PROCHECK[30] program. There is clearly a relatively monotonic increase in $\Delta\sigma^*$ error with the increasing percentage of residues outside the most favorable regions of ϕ,ψ space, and this can be modeled by the exponential curve illustrated in Figure 8. Since the curve passes through the origin, this result suggests that most of the $\Delta\sigma^*$ error seen originates from uncertainties in the ϕ,ψ torsion angles used in the calculations, implying that $\Delta\sigma^*$ values can be used in structure refinement.

For C^{β} and other side chain positions, the results shown in Table 2, as noted above, show a small increase in shielding of helical versus sheet residues, together with an overall ~2.7 ppm increased C^{β} CSA (Ω). This increase is very small and relatively insensitive to ϕ,ψ. However, as might be expected, ^{13}C NMR isotropic chemical shifts of the side chain carbons can be quite sensitive to χ_1 and χ_2, especially in the branched amino acids where the occurrence of multiple γ-gauche-type interactions may contribute to shielding. In the past, we have not considered side chain carbons in any detail, since we thought that the presence of enhanced motion or crystal/solution structural differences might make any successful chemical shift predictions impossible. However, in recent work on several ^{13}C-labeled proteins,[31−33] it has been shown that well-resolved ^{13}C NMR spectra can now be obtained by using fast magic-angle sample-spinning

(30) Laskowski, R. A.; Rullmann, J. A. C.; MacArthur, M. W.; Kaptein, R.; Thornton, J. M. *J. Biomol. NMR*, **1996**, *8*, 477−486.
(31) McDermott, A.; Polenova, T.; Bockmann, A.; Zilm, K. W.; Paulsen, E. K.; Martin, R. W.; Montelione, G. T. *J. Biomol. NMR* **2000**, *16*, 209−219.

Table 4. Compilation of Experimental (Solid-State and Solution) ^{13}C NMR Chemical Shifts and Predicted Shieldings for C^{α}, C^{β}, $C^{\gamma 1}$, $C^{\gamma 2}$, and C^{δ} in Ile18 and Ile19 in BPTI

		δ ^{13}C (ppm)[a]		σ_{calc} (ppm)	
		solution	solid state	X-ray[b]	NMR[c]
Ile 18	C^{α}	60.4	60.2	141.0	139.2
	C^{β}	40.1	39.9	156.9	155.4
	$C^{\gamma 1}$	18.9	19.2	168.1	167.2
	$C^{\gamma 2}$	27.4	28.5	177.2	178.2
	C^{δ}	14.3	14.9	178.9	179.5
Ile 19	C^{α}	61.3	60.2	142.2	143.0
	C^{β}	35.9	34.9	162.7	162.2
	$C^{\gamma 1}$	17.6	19.5	169.3	170.3
	$C^{\gamma 2}$	27.7	27.7	177.7	179.4
	C^{δ}	10.9	10.9	184.1	185.4

[a] From ref 31. [b] Using the X-ray structure 5PTI from ref 34. [c] Using the average solution NMR structure 1PTI from ref 35.

methods. This permits measurement of isotropic ^{13}C NMR chemical shifts for many side chain carbons and, in one case, a comparison with their corresponding solution NMR values, which were found to be very similar.[31] We have now investigated the $^{13}C^{\alpha}$, $^{13}C^{\beta}$, $^{13}C^{\gamma 1}$, $^{13}C^{\gamma 2}$, and $^{13}C^{\delta}$ isotropic chemical shifts in the isoleucine species shown below, in bovine pancreatic trypsin inhibitor (BPTI), where both solution and solid-state spectra and structures are available.[31,34,35]

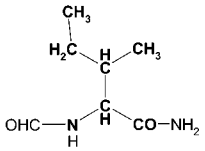

There are two Ile's in BPTI, Ile18 and Ile19. Both are in sheet regions, but they have different side chain (χ_2) conformations.[34] Ile18 has a trans χ_2, whereas Ile19 is present in a gauche (−) form.[34] Using the HF-GIAO methods described above but with an extended locally dense basis (6-311G++(2d,2p) on all carbons of interest (shown in bold above), we computed the C^{α}, C^{β}, $C^{\gamma 1}$, $C^{\gamma 2}$, $C^{\gamma 2}$, and C^{δ} shieldings for both residues. The individual shieldings for each carbon in each residue are shown in Table 4 and are plotted versus the experimental ^{13}C NMR chemical shifts in Figure 9. We show in Figure 9A the ^{13}C NMR shieldings predicted from the crystal structure versus the solid-state NMR chemical shifts, where we find that rmsd = 1.1 ppm, $R^2 = 1.0$, and the slope is −0.84. Essentially the same results are obtained when using the solution NMR shifts (since they are about the same as the solid-state shifts) (Table 4). When using an average solution NMR structure,[35] the rmsd increases to 2.0 ppm, $R^2 = 0.98$, and the slope is −0.90 (Table 4 and Figure 9C). In another protein, cytochrome *c*, we also find good accord between experimental solution ^{13}C NMR shifts[36] and those predicted by using crystallographic results,[37] as shown in Table 5 and Figure 9D, where the rmsd is 1.8 ppm and $R^2 = 0.98$. Overall, these results strongly suggest that isotropic chemical shifts of complex side chains may also be successfully reproduced by using HF-GIAO methods, opening up the possibility of determining, or at least refining, both peptide backbone and amino acid side chain conformations, by using quantum chemical methods.

Table 5. Compilation of Experimental Solution ^{13}C NMR Chemical Shifts and Predicted Shieldings for C^{α}, C^{β}, $C^{\gamma 1}$, $C^{\gamma 2}$, and C^{δ} in Ile35, Ile53, Ile75, and Ile95 in Cytochrome *c*

		δ^{13}C (ppm)[a]	σ_{calc} (ppm)[b] (X-ray)
Ile35	C^{α}	61.5	142.1
	C^{β}	37.9	159.2
	$C^{\gamma 1}$	19.0	175.6
	$C^{\gamma 2}$	29.4	165.8
	C^{δ}	15.9	179.4
Ile53	C^{α}	65.3	135.7
	C^{β}	39.3	157.1
	$C^{\gamma 1}$	17.1	178.9
	$C^{\gamma 2}$	28.4	166.2
	C^{δ}	14.0	179.4
Ile75	C^{α}	59.9	142.8
	C^{β}	38.4	155.0
	$C^{\gamma 1}$	19.1	176.4
	$C^{\gamma 2}$	28.6	168.0
	C^{δ}	13.2	176.9
Ile95	C^{α}	66.2	135.8
	C^{β}	37.2	157.9
	$C^{\gamma 1}$	17.7	178.3
	$C^{\gamma 2}$	31.4	166.2
	C^{δ}	13.1	179.4

[a] The experimental results are unpublished work of C. M. Szabo. [b] The theoretical shieldings were based on the 2YCC cytochrome structure (ref 37).

It also appears that anisotropic shieldings or tensor breadths may play a role in *side chain* structure refinement, since they appear to be sensitive to χ_1, χ_2 but much less so to ϕ,ψ. For example, in earlier work, we measured the C^{β} CSA $\Omega = \delta_{11} - \delta_{33}$ in a tri-alanine hemihydrate and found $\Omega_{expt} = 37.5$ ppm and $\Omega_{calc} = 39.0$ ppm from the shielding surfaces at the relevant ϕ,ψ angles.[24] However, $|\sigma_{33} - \sigma_{11}|$ computed values for helical and sheet geometries were quite close: 32.5 and 38.4 ppm.[11] In the case of more complex amino acid side chains, for example, the Ile considered above, there are, however, considerable variations in Ω from this large value that are similarly not ϕ,ψ-sensitive, but rather, are χ_1, χ_2-sensitive. In ubiquitin, the **mt** conformers have $\Omega = 21$ ppm for both ideal helix ($\phi = -60°$, $\psi = -60°$) and sheet ($\phi = -120°$, $\psi = 120°$) geometries, and the computed $\Omega = \sigma_{33} - \sigma_{11}$ values for C^{γ_1} for the **pt** conformers in helices and sheets are also both 20 ppm. These results are in good accord with a global minimum of $\Omega = 20.5$ ppm measured experimentally by Hong for Ile's in ubiquitin using solid-state NMR.[38] For the **mm** conformer, Ω values of only 12 and 13 ppm are predicted from the calculations and should be measurable experimentally. Moreover, Ω values for $C^{\gamma 2}$ (the other Me group) also vary considerably between **mt** and **pt** (24 vs 14 ppm), again opening up the possibility of deducing side chain Ω information.

Conclusions

The results we have described above are of interest for a number of reasons. First, we have completed computation of the $^{13}C^{\alpha}$ and $^{13}C^{\beta}$ NMR chemical shielding tensors and their orientations for all 20 amino acids in their most popular

(32) Pauli, J.; van Rossum, B.; Forster, H.; de Groot, H. J.; Oschkinat, H. *J. Magn. Reson.* **2000**, *143*, 411−416.
(33) Hong, M. *J. Biomol. NMR* **1999**, *15*, 1−14.
(34) Wlodawer, A.; Walter, J.; Huber, R.; Sjolin, L. *J. Mol. Biol*. **1984,** *180*, 301−329.
(35) Berndt, K. D.; Guntert, P.; Orbons, L. P.; Wüthrich, K. *J. Mol. Biol*. **1992**, *227*, 757−775.
(36) Szabo, C. M.; Sanders, L. K.; Le, H. C.; Chien, E. Y. T.; Oldfield, E. *FEBS Lett.* **2000**, *482*, 25−30.
(37) Berghuis, A. M.; Brayer, G. D. *J. Mol. Biol.* **1992**, *223*, 959−976.
(38) Hong, M. *J. Am. Chem. Soc.* **2000**, *122*, 3762−3770.

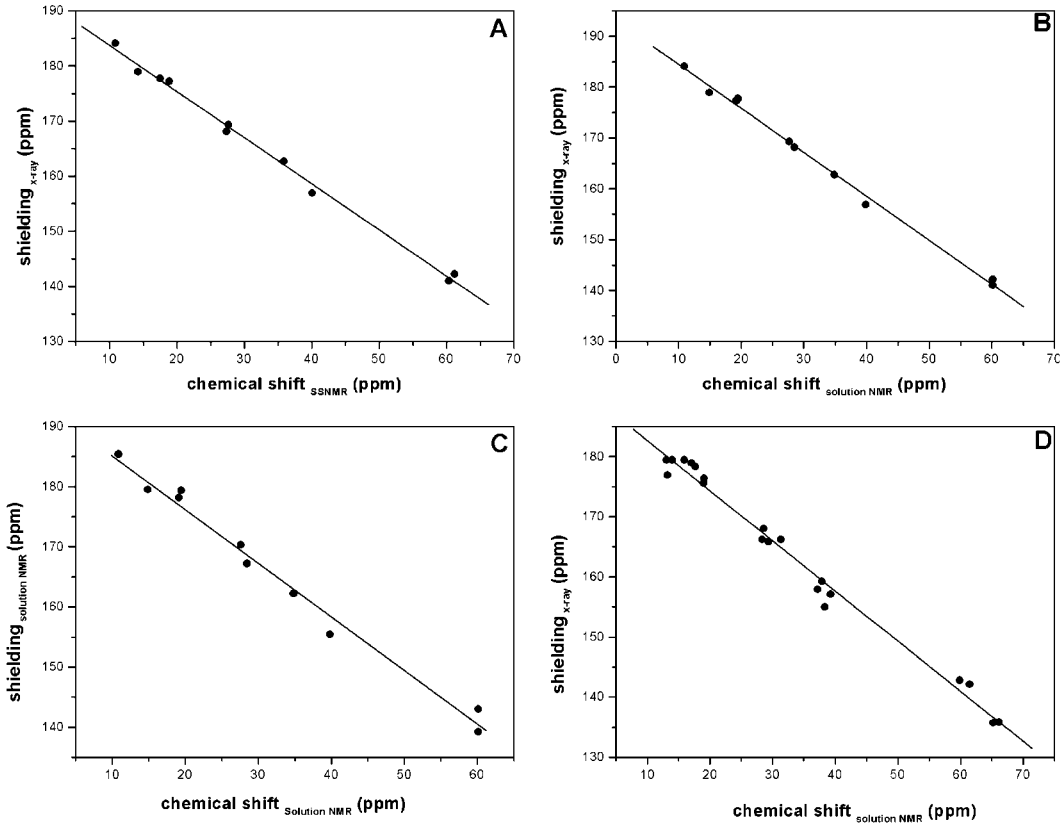

Figure 9. Graphs showing correlations between experimental isotropic chemical shifts, δ, in ppm from TMS and the computed absolute shieldings, σ, for C^{α}, C^{β}, $C^{\gamma 1}$, $C^{\gamma 2}$, and C^{δ} in Ile18 and Ile19 in BPTI (A−C) and Ile35, Ile53, Ile75, and Ile95 in cytochrome *c* (D): (A) experimental solid-state shift/X-ray predicted shieldings (slope = −0.84, *y* intercept = 192.1 ppm, $R^2 = 1.00$, rmsd = 1.1 ppm); (B) experimental solution NMR shift/X-ray predicted shieldings (slope = −0.86, *y* intercept = 193.0 ppm, $R^2 = 1.00$, rmsd = 1.1 ppm); (C) experimental solution NMR shift/solution NMR structure predicted shieldings (slope = −0.90, *y* intercept = 194.6 ppm, $R^2 = 0.98$, rmsd = 2.0 ppm); (D) experimental solution NMR shift/X-ray predicted shieldings (slope = −0.83, *y* intercept = 191.0 ppm, $R^2 = 0.98$, rmsd = 1.8 ppm).

conformations found in proteins. Second, examination of these results has led to the unexpected observation that only in the β-branched amino acids valine, isoleucine and threonine, are there likely to be very large differences between helical and sheet $^{13}C^{\alpha}$ CSA (Ω) values. Third, our results clearly show that the very large differences between helical and sheet $^{13}C^{\alpha}$ CSAs ($\Delta\sigma^*$) determined from solution NMR are overwhelmingly dominated by changes in tensor orientation, not by changes in the actual magnitudes of the principal components of the chemical shielding tensor. Fourth, we have obtained $^{13}C^{\alpha}$ shielding tensor orientation surface results that confirm the dominance of σ_{22} in shielding along the C−H bond vector in helical domains but the dominance of σ_{11} in sheet residues. Fifth, by using this tensor orientation information we have evaluated $\Delta\sigma^* = \sigma_{orth} - \sigma_{par}$ values for numerous residues in calmodulin and ubiquitin. The rms deviations between experimental and predicted $\Delta\sigma^*$ values for ubiquitin are quite small, ~2.7 ppm, for an average solution NMR structure and ~3.6 ppm for a crystal structure, whereas those for the larger protein calmodulin are much larger. The $\Delta\sigma^*$ errors are a function of the ϕ,ψ errors, as assessed by the PROCHECK program, which suggests that $\Delta\sigma^*$ can be used as a refinement tool. Sixth, although the $^{13}C^{\alpha}$ tensor orientations change considerably between helical and sheet residues, there are only very minor differences in the $^{13}C^{\beta}$ tensor magnitudes and orientations for all 20 amino acids. Seventh, using HF-GIAO methods, we have been able to successfully predict both backbone and side chain isotropic chemical shifts: $^{13}C^{\alpha}$, $^{13}C^{\beta}$, $^{13}C^{\gamma 1}$, $^{13}C^{\gamma 2}$, and C^{δ} for the two isoleucine residues in BPTI and the four in a cytochrome *c*, opening up the possibility of using ^{13}C NMR chemical shifts (and shift anisotropies) to refine amino acid side chain conformations in proteins using quantum chemistry. Taken together, these results suggest that the availability of shielding surfaces for each amino acid, together with the increasing availability of both solution and solid-state shift and shielding tensor information, should open up new areas for structure refinement and determination using the ^{13}C NMR chemical shift property.

Acknowledgment. This work was supported by the United States Public Health Service (NIH grant GM-50698) and by the National Computational Science Alliance (NSF grants MCB 000018N and MCB000020N). We thank Christina Szabo for providing the cytochrome *c* assignments prior to publication.

Supporting Information Available: Shielding and tensor orientation data (112 pages, print/PDF) for all 20 amino acids. This material is available free of charge via the Internet at http://pubs.acs. org.

JA011863A